ENA (E > 5 keV) Images from Cassini and Voyager "ground truth": Suprathermal Pressure in the Heliosheath

S. M. Krimigis[a,b], D. G. Mitchell[a], E. C. Roelof[a], and R. B. Decker[a]

[a]*Applied Physics Laboratory, Johns Hopkins University, Laurel, MD 20723, USA*
[b]*Office for Space Research and Technology, Academy of Athens, 11527 Athens, Greece*

Abstract. Maps of energetic neutral atoms (ENA) of the heliosphere from Cassini [1] have been constructed spanning the energy range ~ 5 ≤ E ≤ 55 keV, and show a "Belt" in the sky of ~ 100° FWHM. Similarly, maps < 6 keV have been obtained by the IBEX mission [2] and show a "Ribbon" that is narrower than the Belt and inclined to it in both ecliptic latitude (~25°) and longitude (~30°). The overlap in energy between Voyager ions [3] and Cassini ENA intensities (averaged over the ENA line of sight) enables us to deduce ion fluxes in the heliosheath, thus providing a continuous spectrum 5 ≤ E ≤ 4000 keV. These measurements are then used to estimate the local partial pressure over this energy range (~ 0.1 pPa), suggesting β >25 [4] and the thickness of the heliosheath (~ 50 AU). Using a simulated PUI distribution [5], we estimate the E < 6 keV contribution to be ~ 0.12 pPa. The balance of the non-thermal pickup ion (PUI) pressure against the stagnation pressure of the interstellar plasma and the local interstellar magnetic field (ISMF) at the nose of the heliopause implies an upper bound on the ISMF of ~0.64 nT

Keywords: Heliospheric termination shock, Energetic neutral atoms, Non-thermal plasma, interstellar magnetic field
PACS: 96.50.Ek Heliopause and solar wind termination; 96.50.Zc Neutral particles; 96.50.Xy Heliosphere/interstellar medium interactions

INTRODUCTION

The two Voyager (V1, V2) spacecraft have been traversing the heliosheath for the past few years, transmitting information on the charged particles and fields environment. Intensities of energetic (> 28 keV) ions, on average, have been remarkably similar at the two spacecraft, even though they are separated by a distance > 130 AU, at latitudes of ~ 35° (V1) and -30° (V2) [6]. These measurements, however, are in situ and the broader context of the heliosheath remained unknown until the recent ENA images obtained by the Cassini Magnetospheric Imaging Instrument (MIMI) Ion and Neutral Camera (INCA) sensor [1] and the IBEX mission [2]. Relating the ENA spectrum in the image pixel containing V2 to the ion source population (5-55keV) and matching it to the overlapping 30-3500keV ion spectrum measured *in situ* by V2 enables the computation of the non-thermal pressure associated with PUIs at E > 5 keV. Adding in an estimate of the non-thermal pressure at < 5 keV as well as the thermal plasma pressure measured by the plasma instrument on V2, we can estimate the level of the interstellar magnetic field necessary to contain the hot heliospheric plasma. A by-product of this procedure is an estimate of the thickness of the heliosheath in the direction of V2.

THE ENA "BELT" AND "RIBBON"

The most remarkable aspects of the ENA images are the unexpected spatial distribution of the emissions and the substantial differences in the shape of low (~1 keV, [7]) and high (> 5 keV, [1]) energies. Figure 1 shows the Cassini/INCA ENA celestial sphere plotted in ecliptic coordinates, with the IBEX "ribbon" sketched in. There are emissions both from the direction of the interstellar flow (Nose) as well as the opposite (Tail), plus strong intensities through the north and south ecliptic poles. Both Voyagers are located within the belt, north and south of the ecliptic equator. Note that the belt straddles the galactic equator.

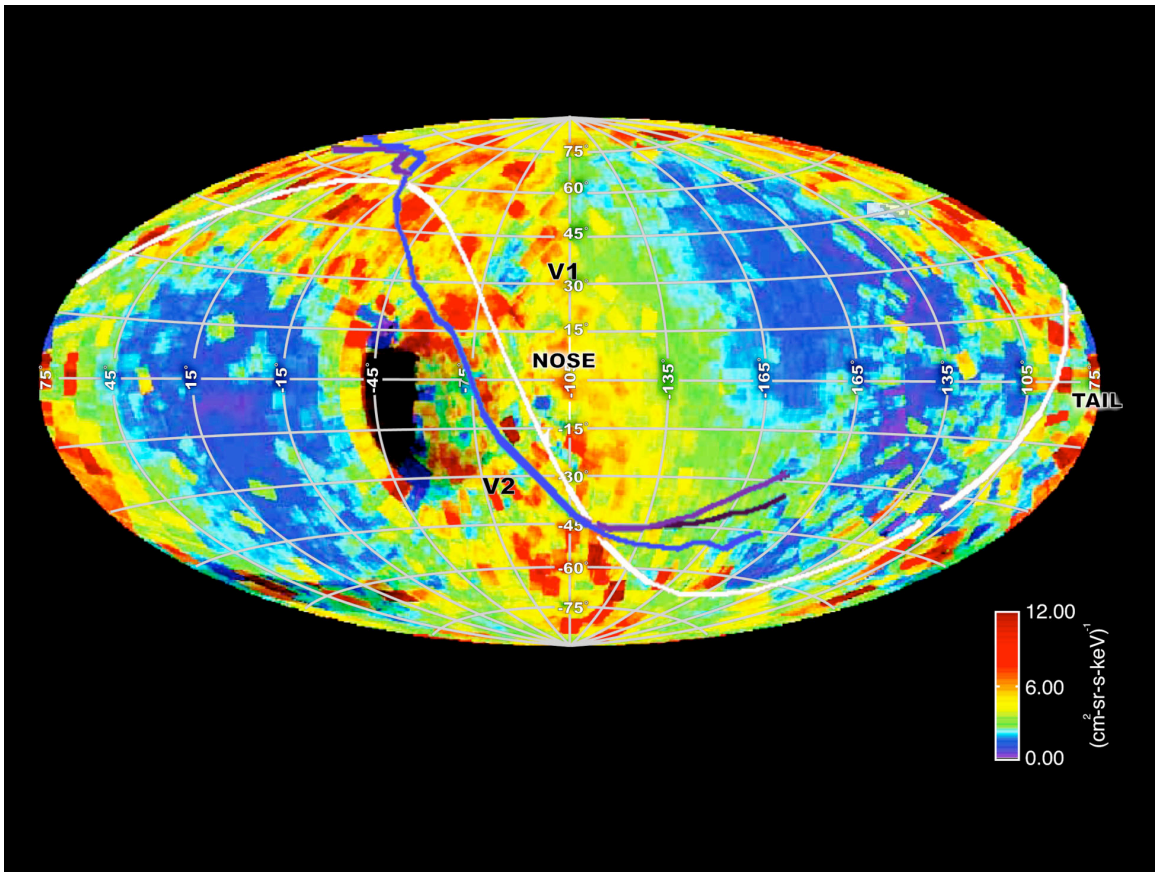

FIGURE 1. Image of heliospheric ENA in the range 5.2-13.5 keV obtained with Cassini/ MIMI/INCA plotted in ecliptic coordinates. The location of local interstellar flow (Nose), and its opposite (Tail), and the positions of Voyager 1, 2 in the heliosheath are marked. The thick white line shows the galactic equator. The blue line shows the centerline of the IBEX ribbon (2) and the magenta and black lines at low (<–30°) and high (> 60°) latitudes indicate the ribbon's range at different energies.

Although not clear from this figure, the ribbon forms a near circle [7] of radius 72° centered on ecliptic (λ, β) = (221°, 39°), and its normal is inclined relative to that of the belt. The Ribbon is relatively narrow at ~ 1 keV and becomes broader at higher energies [2]. The schematic in Fig. 2 is an attempt at depicting the relative orientation of the low energy Ribbon and the high energy Belt. Here the width of the heliosheath has been estimated as ~ 50 AU [1], while the Ribbon is shown as extending to > 200 AU [8]. At this point, the radial extent of the ribbon is the subject of extensive debate [2, 9, 10].

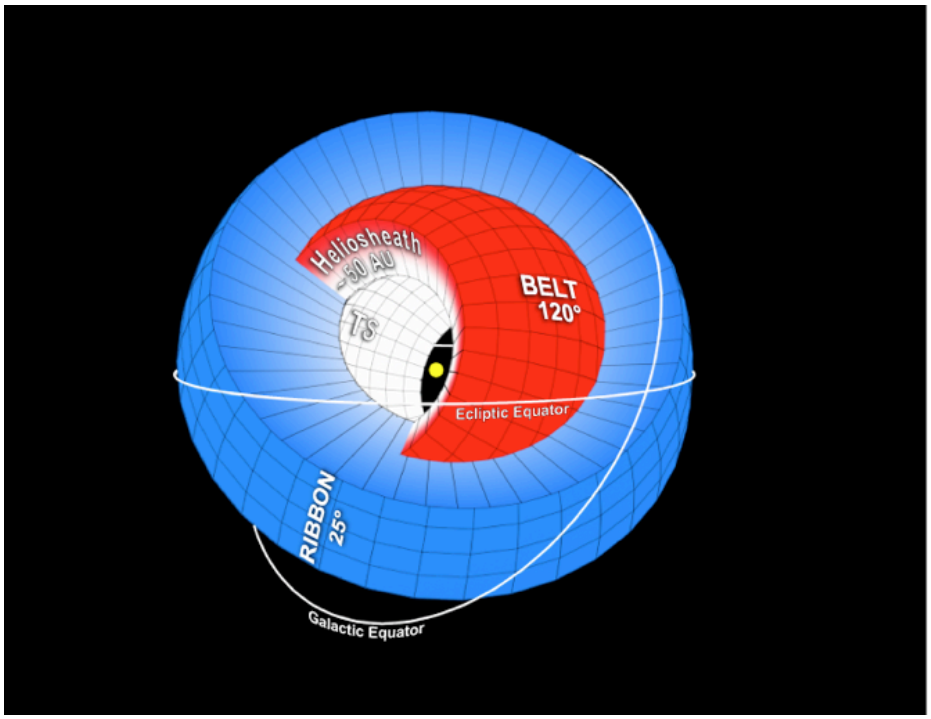

FIGURE 2. Schematic of the radial and latitudinal extent of the Belt and the Ribbon as seen from outside the heliosphere. The Sun is at the center (yellow), the solar wind proper is black inside the Termination Shock (TS) set at ~ 90 AU, the heliopause at ~ 140 AU is the estimated radial extent of the Belt, while the Ribbon is shown as extending from the TS to well beyond the heliopause, allowing for the present range of estimates on its extent. The galactic and ecliptic equators are indicated.

ENERGY SPECTRA IN THE HELIOSHEATH

The presence of the two Voyagers in the heliosheath provides "ground truth" measurements on the actual intensities of protons (and heavier ions under certain assumptions) so that one can relate these to the ENA line-of-sight intensities observed inside the heliosphere without needing assumptions on pitch angle distributions, extinction factors, etc., provided that there is energy overlap in the respective data channels. A partial overlap exists between the Voyager 1, 2 Low energy Charged Particle (LECP) ion instrument ([11], $28 < E < 4000$ keV) and the Cassini ENA INCA sensor ($5.2 < E < 55$ keV) used to obtain the heliosphere images. There is also a plasma instrument (PLS) on Voyager 2 [12] that covers the nominal range ~10 eV $< E < 6$ keV, but is only sensitive to $E < 1$ keV in the heliosheath. Thus there is little overlap between PLS and the IBEX ENA sensors.

Using INCA images similar to that of Fig. 1 it is possible to construct ENA spectra for various locations in the sky. Spectra from selected areas shown in Fig. 3 (lower grouping) illustrate the range of intensities from minima to maxima, a factor of ~ 6 for the lowest energy channel. The differential intensity varies as $E^{-3.5}$ and it is nearly independent of location in the sky. A more detailed spectral map (not shown) reveals that this is a general result throughout the celestial sky. The V1 and V2 spectra measured in the heliosheath [3] on the right exhibit the well-known $E^{-1.5}$ form. A most remarkable aspect of the deduced proton spectra in the heliosheath is that the higher energy points fit smoothly onto the V2 and V1 spectra, but are substantially steeper as the energy decreases, as some of the simulations predict [5].

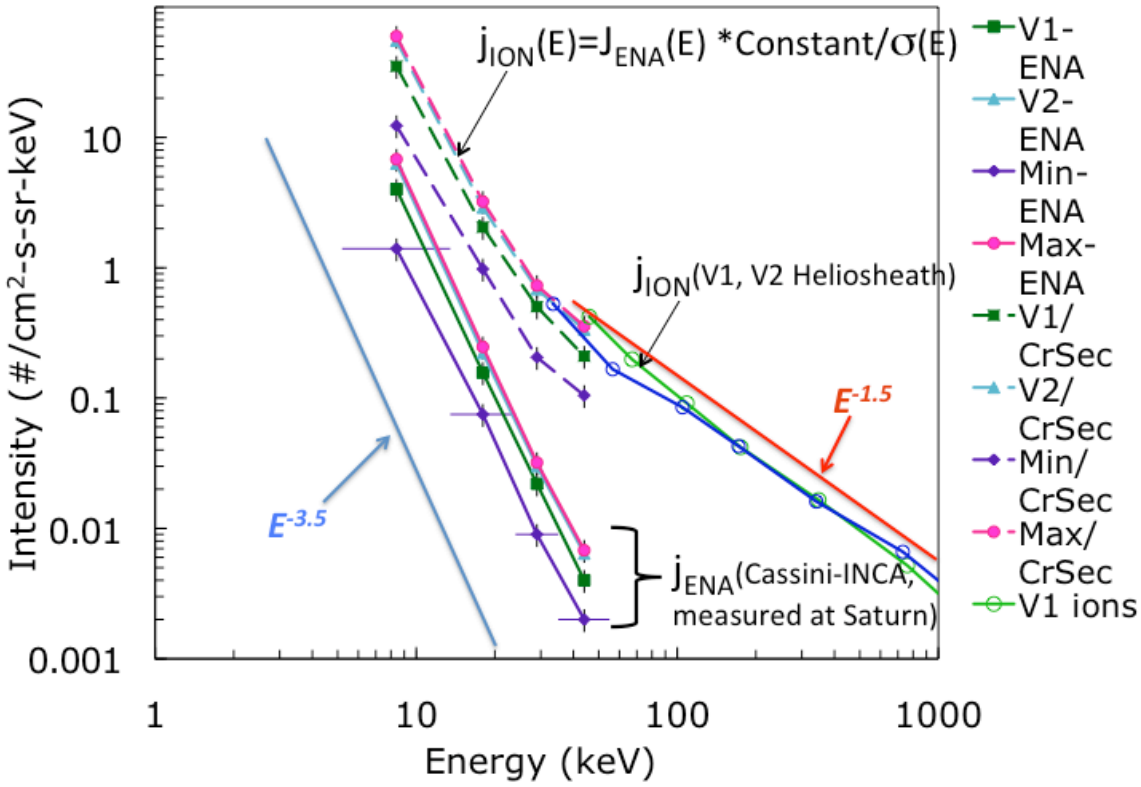

FIGURE 3. ENA spectra of INCA data over the energy range 5.2-55 keV (lower grouping) from selected locations shown in Fig.1, and deduced proton spectra (upper grouping). Laboratory charge exchange cross sections for protons on hydrogen are used for each channel in a medium with density 0.1 cm^{-3}, with the 44 keV channel normalized to the in situ intensity measured by Voyager 2 at ~ 90 AU. The normalization factor is used to estimate the size of the region beyond the TS at ~ 50 AU.

A by-product of this procedure is an estimate of the heliosheath thickness in the V2 direction. The line-of-sight intensity j_{ENA}, ion intensity j_0, local hydrogen density in the heliosheath n_0, charge exchange cross section σ^{10}, and the average radial interval L_{ion} beyond the TS where the product $n_0 j_0$ is relatively constant are related [1] by the expression

$$j_0 = j_{ENA}/(\sigma^{10} n_0 j_0 L_{ion})$$

In Fig. 3 we multiplied the ENA intensity at 44 keV (geometric mean of highest energy INCA channel) by a factor of 80 in order to obtain $j_0 = 0.335$ that fits on the V2 spectrum between the 33.5 and 56.5 keV points (upper set of curves). Assuming $n_0 = 0.1(\pm 20\%)$ cm^{-3}, we deduce that $L_{ion} = 54$ (+30, −15) AU, where the errors include uncertainties associated with the laboratory-measured value of σ^{10}. We adopt 50 AU as a nominal value for the width of the heliosheath. Note that we *deduced* the value of L_{ion} by matching the INCA-inferred ion spectrum to the *in situ* measured V2 spectrum; at no point in our analysis in this paper do we ever need to *assume* a value for L_{ion} or to invoke any model for ion intensities in the heliosheath.

PUI PRESSURE AND THE INTERSTELLAR MAGNETIC FIELD

The V1 and V2 crossings of the TS revealed that PUI pressure in the heliosheath was significantly higher than magnetic field pressure, as shown in Fig. 4. The pressure at V2 in particular (lower panel) at E > 28 keV was 0.023 pPa at TS crossing and peaked at 0.036 a few days later, i.e. *i.e.,* just this partial pressure alone was ~5 times the measured magnetic pressure ($B^2/2\mu_0 \sim 0.004$ pPa for B = 0.10 nT). The ion PUI spectra shown in Fig. 3 implies a pressure over the energy range 8-44 keV of 0.077 pPa, giving a partial pressure 5-3500keV of 0.10 pPa. Neglect overlap.

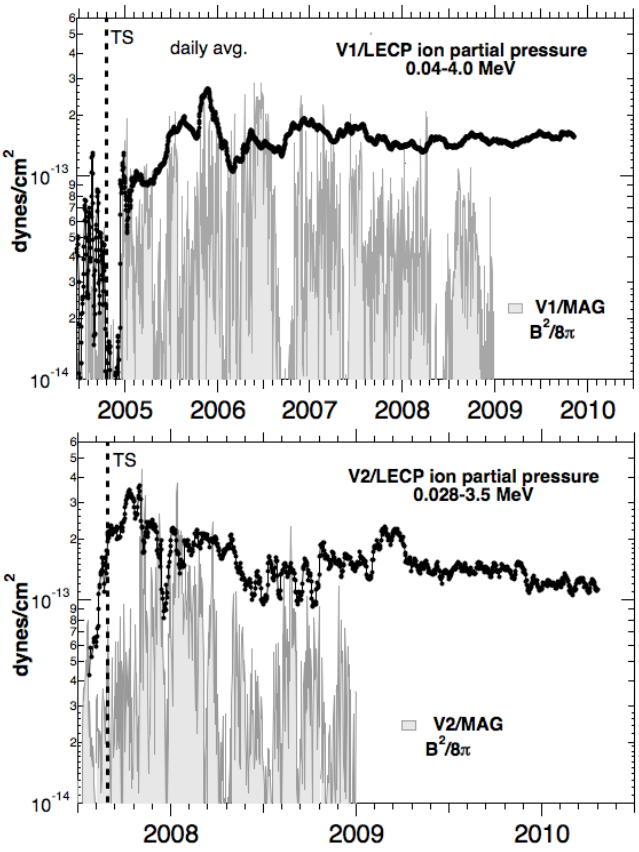

FIGURE 4. Time history of the pressure of energetic protons just upstream and also downstream of the TS for Voyager 1 (top) and Voyager 2 (bottom) is plotted in the indicated energy intervals. The in situ magnetic pressure is shaded in. The heliosheath is consistently β > 1, even counting only the partial pressure due to ions E>28 keV.

The only component of the pressure not measured directly is the E < 6 keV, i.e. the energy range of the IBEX images. An estimate for this partial pressure is provided by a self-consistent, two-dimensional hybrid simulation [5] that is able to reproduce the observed intensity of the $E^{-1.5}$ non-thermal tail of ions with E > 28 keV at V2 downstream of the TS and is found to be ~ 0.121 pPa. This compares well with the IBEX estimate of 0.15 pPa at the V2 pixel [7] if one assumes L_{ion}= 50 AU. Thus the overall (isotropic) pressure in the heliosheath immediately downstream of the TS is $P_{total} = p_{th} + p_{st1} + p_{st2} + p_{ep} + p_{mag} = (0.005+0.121+0.077+0.023+0.004) = 0.230$ pPa. In addition, there is also the ram pressure of the downstream thermal ions measured by V2 of ρV^2~0.075 pPa [13], but this must be "book-kept" separately (below).

Finally, we utilize these pressure values in order to estimate the magnitude of the interstellar magnetic field (ISMF). We think it reasonable to presume that the pressure at V2 of ~ 0.23 pPa is similar to that at V1 (Fig. 4) and is therefore characteristic of the nose portion of the termination shock because of the remarkable agreement of the intensities in the $E^{-1.5}$ tails above ~ 28 keV (despite the separation of the two spacecraft by 130 AU!). We will assume that the same pressure is carried out to the heliopause. True, there will be some adiabatic cooling and charge-exchange loss en route (although this could be compensated by "ubiquitous" compressional acceleration [14], so our estimate of the ISMF should be considered an upper limit. The thermal ram pressure (if it persists from

the TS to the heliopause) will not affect the force balance there, because (by definition) there is no flow across an ideal heliopause. We estimate the pressure at the Nose of the heliopause due to stagnation flow of the interstellar plasma flow in the approximation of slow incompressible flow (Bernoulli's equation). We have also neglected the magnetic tension stress ($\mathbf{B}\cdot\nabla\mathbf{B}/\mu_0$) produced by the draping of the field around the heliopause, so again, our estimate should yield an upper limit on the ISMF. Then $\rho V^2/2+P+B^2/2\mu_0 \cong$ constant along a flow streamline. In the interstellar medium the thermal pressure $(nkT)_{IS}$ = 0.010 pPa while $(\rho V^2/2)_{IS}$= 0.0565 pPa if we assign a plasma density of 0.1 cm^{-3}.

The required magnetic pressure outside the heliopause should therefore be $P_{ISMF}=P_{total}-(\rho V^2/2+nkT)_{IS}=0.230-0.0665=0.1635$ pPa. This is 3.5 times the stagnation pressure of the interstellar flow, so although the flow effects should affect the structure of the nose heliopause somewhat, the effects of the ISMF should dominate. Our upper limit for the ISMF value is $B_{IS} \sim 0.64$ nT, which is significantly larger than the commonly assumed value of 0.25 nT. We note, however, that estimates for the magnitude of the ISMF as high as 0.7 nT [15] are in the literature. In fact, models used to explain the observed asymmetry between the north (94 AU) and south (84 AU) asymmetry of the TS, can only do so with large values of ~ 0.4 nT [16] and 0.35-0.55 nT [17] for the ISMF. We conclude that the non-thermal PUI pressure measurements, despite some uncertainties, point to a stronger ISMF than assumed heretofore.

ACKNOWLEDGEMENTS

We are grateful to Martha Kusterer and John Ajello for programming and display assistance. The work at JHU/APL on Cassini/MIMI was supported by NASA under contract NAS5-97271 and NNX07AJ69G**.** The work on the Voyager Interstellar Mission was supported under NASA Contact NNX07AB02G to the Johns Hopkins University.

REFERENCES

1. S. M. Krimigis et al, *Science, 326*, 971, (2009).
2. D. J. McComas et al, *Science, 326*, 959, (2009).
3. R. B. Decker et al, *Solar Wind 12*, 25 June, (2009).
4. L. F. Burlaga et al, *J. Geophys. Res., 114*, A06106, (2009).
5. J. Giacalone and R. B. Decker, *The Astrophysical Journal, 710*:91–96, (2010).
6. R. B. Decker et al, this volume
7. H. O. Funsten *et al.*, *Science,* **326**, 964-966 (2009).
8. J. Heerikhuisen et al, *ApJ Lett., 708*:L126–L130, (2010).
9. H. Kucharek et al, this volume
10. V. A. Florinski, *Astrophys. J., 718*, 1-7, (2010).
11. S. M. Krimigis, T. P. Armstrong, et al., *Space Science Rev.* **21**, 321 (1977).
12. J. D. Richardson, J. C. Kasper, C. Wang et al., *Nature* **454**, 63 (2008).
13. E. C. Roelof et al, this volume
14. L. A. Fisk, and G. Gloeckler, *Adv. Space Res., 43*,1471, (2009).
15. D. Cox, and L. Helenius, *ApJ. 583*, 205–228 (2003).
16. N. Pogorelov, et al, *ApJ. 695*, L31, (2009).
17. M. Opher et al, *Nature 462*, 1036 (2009).